Journal of Catalysis **194,** 250–265 (2000)
doi:10.1006/jcat.2000.2943, available online at http://www.idealibrary.com on IDEAL®

The Selective Catalytic Reduction of Nitric Oxide with Methane over La_2O_3–CaO Systems: Synergistic Effects and Surface Reactivity Studies of NO, CH_4, O_2, and CO_2 by Transient Techniques

C. N. Costa, T. Anastasiadou, and A. M. Efstathiou[1]

Department of Chemistry, University of Cyprus, P.O. Box 20537, CY 1678 Nicosia, Cyprus

Received January 12, 2000; revised May 30, 2000; accepted May 31, 2000

Dispersing La_2O_3 crystallites in a 5 wt% La_2O_3–CaO mixed oxide system significantly enhances the intrinsic rate of NO reduction by CH_4 in the presence of 5% O_2 at 550°C compared to pure La_2O_3 and CaO phases. A synergistic effect between La_2O_3 and CaO crystallites due to doping of lanthana with Ca^{2+} ions at 800°C is largely responsible for the observed catalytic behavior. Support of this view was provided by photoluminescence studies and a large number of transient experiments for determining the surface reactivity of *x* wt% La_2O_3/CaO (*x* wt% = 0, 5, 80, 100) solids toward NO, CH_4, O_2, and CO_2. The intrinsic site reactivity of the 5 wt% La_2O_3–CaO system at 550°C (TOF = 6×10^{-3} s^{-1}) competes favorably with that of other similar oxides for the same reaction reported in the literature. X-ray diffraction (XRD) and scanning electron microscopy (SEM) techniques have been used for crystal phases and particle morphology characterization of the *x* wt% La_2O_3/CaO mixed oxide system. The information obtained from the XRD measurements was related to that obtained from the surface transient reactivity studies. By the addition of La_2O_3 crystallites to CaO crystallites in a wet mixing procedure followed by calcination in air at 800°C, results in dramatic changes in the chemisorptive properties (amount and bond strength) of NO, O_2, and CO_2 compared to the case of pure oxide phases. Pretreatment of the catalyst surface with H_2 or CH_4 was found to strongly affect the amount of NO chemisorption and the kinetics of its desorption. These alterations were found to strongly depend on catalyst composition.

Key Words: **lanthana; calcium oxide; NO TPD; O_2 TPD; CO_2 TPD; NO reduction by CH_4; transient methods.**

1. INTRODUCTION

Much research related to the selective catalytic reduction of NO by hydrocarbons (HC-SCR) was undertaken and reported in the literature since the pioneering work of Held *et al.* (1) and Iwamoto (2). Recently, a thorough review paper on the current state of research on lean-NO_x catalysis has appeared (3). Three main groups of active catalysts are mentioned for the HC-SCR process: zeolites, metal oxides, and noble metals. Vannice and his co-workers (4–9) first demonstrated that certain metal oxides, active for the oxidative coupling of methane (OCM) reaction could be considered as potential materials for the HC-SCR process. These catalysts (i.e., La_2O_3 and Sr/La_2O_3) present certain advantages compared to zeolites and supported noble metals, i.e., they are inexpensive and they have a relatively high stability under lean-NO_x reduction conditions. On the other hand, one of the drawbacks of such metal oxides is their low surface area, compared to zeolite-based catalysts, and rates of N_2 formation on a gram-basis appear to be an order of magnitude lower than those obtained on zeolite-based catalysts. However, specific activities reported for La_2O_3 (5), Sr/La_2O_3 (4), and CaO (10) are found to be similar or higher. Based on these results, certain metal oxides can be seen as potential catalysts of the HC-SCR process in the 500–700°C range, if ways are found to increase their rate per gram-basis.

Recently, Shi *et al.* (9) have shown that dispersing La_2O_3 on δ- or γ-Al_2O_3 significantly enhanced the rate of NO reduction by CH_4 in the presence of oxygen as compared to unsupported La_2O_3. Fokema and Ying (11) have recently reported on the $CH_4/NO/O_2$ reaction on nanocrystalline Y_2O_3, Sc_2O_3, and La_2O_3 oxides. It was found that Y_2O_3 performs extremely well in the 400–650°C range and has comparable catalytic activity to that of Co-ZSM5. The large worldwide reserves of natural gas and the availability of CH_4 at gas-fired power plants make methane an attractive reductant for many applications.

In our laboratory, we have initiated a research program concerning the use of certain metal oxides, including perovskite-type materials, as potential catalysts for the selective reduction of NO by hydrocarbons in the presence of excess oxygen. We have recently reported catalytic and kinetic results for the $NO/CH_4/O_2$ reaction on pure CaO (10) and mixed oxidic/perovskitic systems of La–Sr–Ce–Fe–O composition (12). The present work concerns catalytic and transient reactivity studies on the *x* wt% La_2O_3/CaO mixed-oxide system for the $NO/CH_4/O_2$ (lean-NO_x) reaction. The

[1] To whom correspondence should be addressed.

0021-9517/00 $35.00

choice of study of the La_2O_3/CaO system lies in the fact that La_2O_3 (4) and CaO (10) alone proved to be among the most active and selective rare-earth and alkaline-earth metal oxides for the above-mentioned reaction (4–10). A systematic variation of La_2O_3 content in the x wt% La_2O_3/CaO system revealed the existence of a synergistic effect that is dependent of reaction temperature (13). Catalytic, kinetic, and photoluminescence studies performed on the present mixed-oxide system for the $NO/CH_4/O_2$ reaction will be reported elsewhere (13).

In the present work, various bulk and surface characterization studies have been conducted in order to obtain fundamental information about the intrinsic reasons that make La_2O_3 and CaO phases cooperate toward an enhanced catalytic activity. X-ray diffraction (XRD) analyses were performed to probe for the kinds of crystal phases present in the La_2O_3/CaO mixed-oxide system, while scanning electron microscopy (SEM) was used to probe for the morphology of the particles of each of the solid materials investigated. Various kinds of transient experiments were conducted in order to study the reactivity of the surface of each of these catalysts with NO, CH_4, O_2, and CO_2. These included (a) temperature-programmed desorption (TPD) of NO, O_2, and CO_2 in He flow, (b) temperature-programmed surface reaction (TPSR) of preadsorbed NO in CH_4/He and O_2/He flow, and (c) transient isothermal desorption of NO in He flow followed by TPD after $NO/CH_4/O_2$ reaction. The latter allowed the measurement of surface adsorbed NO present under $NO/CH_4/O_2$ reaction conditions.

2. METHODS

2.1. Catalyst Preparation

The mixed metal oxides used in the present work were prepared as follows. Weighted amounts of CaO (Aldrich, 99.9%) and La_2O_3 (Aldrich, 99.999%) corresponding to the desired composition were placed in a glass beaker containing deionized water and heated at 60°C under continuous stirring. After about 90 min of stirring, the slurry obtained was dried at 120°C for 24 h. The dried material was grounded and then placed in an oven in which the temperature was raised stepwise to 800°C. The material was kept at 800°C for 5 h and then cooled in air to room temperature.

2.2. Catalyst Characterization

The specific surface areas of the catalysts were measured using the BET method (Micromeritics 2100E Accusorb) with N_2 as the adsorbate gas. X-ray powder diffraction patterns of the x wt% La_2O_3/CaO solids were obtained after calcination at 800°C using a Philips 1830/40 diffractometer with Cu$K\alpha$ radiation ($\lambda = 1.5415$ Å) and Ni filter 0.4 incoming slit. The surface morphology of the catalysts was examined through a JEOL JSM 5200 scanning electron microscope using a voltage of 25 kV. Powdered specimens were spread on the SEM slabs and sputtered with gold.

2.3. Catalyst Performance and Surface Reactivity Studies by Transient Methods

The flow system used for performing catalyst testing and various kinds of transient experiments is described in Fig. 1. Thermal mass-flow control (MFC) valves (MKS Instruments, Model 247C) were used to prepare *in situ* a given gas mixture. Good mixing of the gas streams was achieved by using small chambers of about 3 ml, the entrances of which were machined in such a way to create local mixing (based on Peclét number). The 4-port chromatographic switching valve V_6 was used to create step concentration functions to the reactor, while the 6-port chromatographic switching valve V_5 was used to deliver pulses to the reactor. Both V_6 and V_5 valves were driven by electric actuators (0.2 s response time). In Fig. 1 it is shown that the gas stream selected by valve V_6 is directed toward a 6-port switching valve, V_3. The bypass loop on this valve is made of exactly the same tubing and fittings as those leading to the reactor. A step change of the feed gas via the V_6 valve bypass the reactor to the mass spectrometer describes the forcing function of the system and accounts for all the backmixing and electronic delays outside of the reactor (14, 15).

The microreactor used in the present work consisted of two 4.0 mm i.d. sections of quartz cylindrical tubes. These served as inlet and outlet to and from a quartz cell (cylindrical shape) of 8.0 mm i.d. (nominal volume 2 ml). A small furnace (cylindrical shape, Thermcraft, Inc.) controlled by a programmable temperature controller (JUMO dTRON 08.1) provided heating of the reactor. The temperature of the catalyst was measured by a 'K'-type thermocouple placed within a quartz capillary well in the entrance of the catalyst bed. Quartz wool was placed at both sides of the catalyst bed to fix the solid sample in place.

For catalytic measurements, 0.2 g of catalyst in powder form were loaded into the reactor. The feed stream consisted of 2000 ppm NO, 6700 ppm CH_4, 5% O_2 and He as balance gas. The total gas flow rate was 50 scc/min yielding a GHSV of $\sim$20000 h^{-1}. Nitrogen reaction rates were calculated from the product analyses using the differential reactor approximation. Rate (mol g^{-1} s^{-1}) $= N_T.y_i/W$, where N_T is the total molar flow rate (mol/s), y_i is the molar fraction of component i, expressed in ppm $\times 10^{-6}$, and W is the weight of the catalyst (g). For the present catalytic system, CH_4 reacts with NO and O_2 according to the competitive reaction scheme

$$2NO + CH_4 + O_2 \rightarrow N_2 + CO_2 + 2H_2O \quad [1]$$

$$CH_4 + 2O_2 \rightarrow CO_2 + 2H_2O. \quad [2]$$

The selectivity, α, for reduction of NO by CH_4 to N_2, i.e., the ratio of the consumption rate of CH_4 for the NO reduction

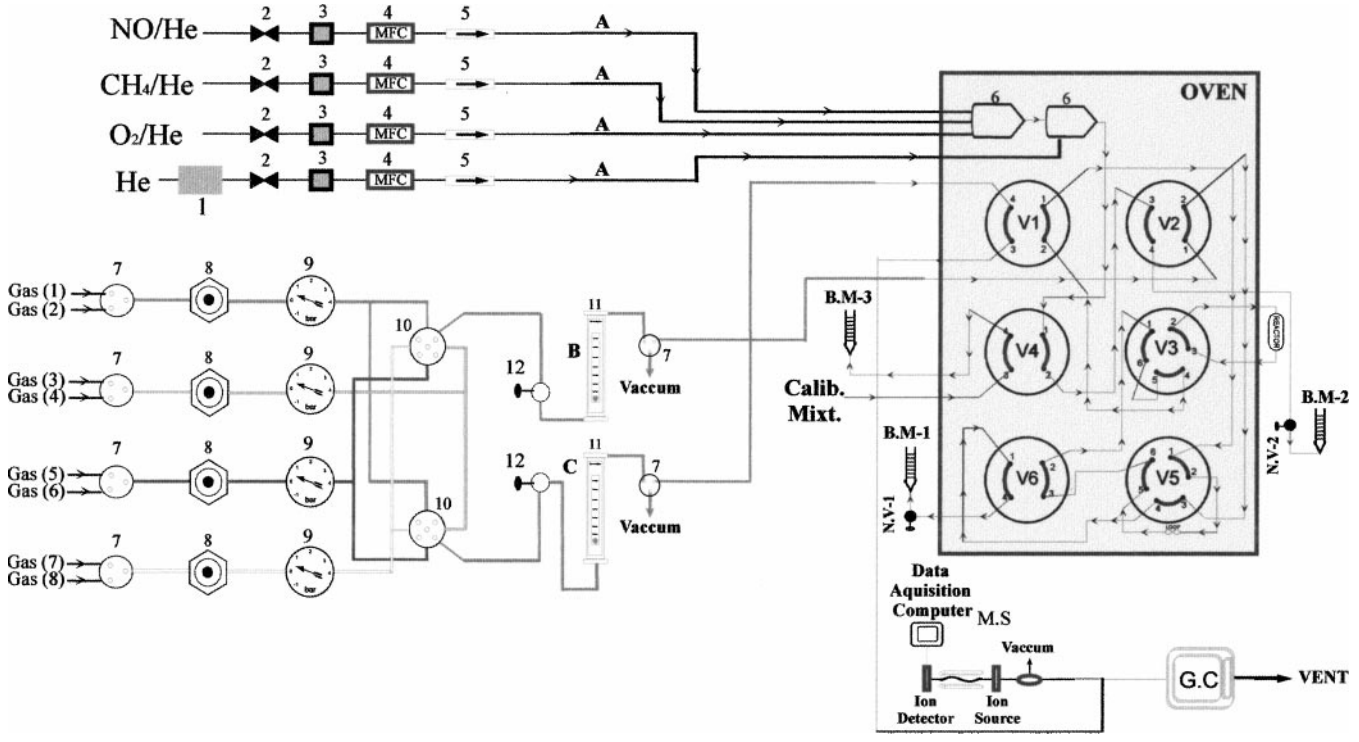

FIG. 1. Schematic diagram of a transient flow system: (1) water and oxy-traps, (2) ON/OFF valve, (3) filter (1 μm), (4) mass flow control valve, (5) check valve (1 psia), (6) mixing chamber (~3 ml), (7) 3-way ball valve, (8) pressure regulator, (9) pressure gauge, (10) 5-way ball valve, (11) rotameter, (12) flow-control valve, B.M. (bubble meter), N.V. (needle valve), V_1, V_2, V_4, V_6 (4-way chromatographic switching valves), V_3, V_5 (6-way chromatographic switching valves), G.C (gas chromatograph), M.S. (mass spectrometer).

(reaction [1]) to the total consumption rate of CH_4 (reaction [1] + reaction [2]) is calculated as previously reported (10).

In all TPD and TPSR experiments, 0.2 g of catalyst (~0.1 mm particle size) and 30 scc/min total gas flow rate were used. All lines between the outlet of reactor and the inlet capillary of MS, including also the latter, were held at 120°C. No gas phase reaction between NO and O_2 to form NO_2 in these lines was detected by mass spectrometry. The reactor effluent was analyzed with a GC (HP 5890A) equipped with molecular sieve 5A and Porapak Q chromatographic columns coupled to an on-line quadrupole mass spectrometer equipped with a fast response inlet capillary/leak valve system (SVI 050, Balzers). Calibration of the gaseous responses obtained was carried out using standard mixtures. For MS analyses, mass numbers (m/z) used were: 15, 28, 30, 32, 44, and 46 for CH_4, N_2, NO, O_2, CO_2 (or N_2O), and NO_2, respectively. Cracking coefficients of a given component required for quantitative analysis were determined based on a mixture of that component in He gas.

The standard pretreatment of a fresh sample consisted of a 4-h initial calcination in flowing dry air at 800°C followed by a He purge at 800°C for 15 min, followed by cooling of the sample to the appropriate temperature for the subsequent experiment. Table 1 describes in detail the necessary sequence of steps performed for each kind of transient experiment presented in this work. The step under which measurements by on-line mass spectrometry were recorded is underlined.

3. RESULTS

Catalyst Characterization

3.1. BET Surface Areas

The specific surface areas (m^2/g) of the x wt% La_2O_3/CaO mixed-oxides evaluated according to the measured nitrogen isotherm at 77 K ($P/P_o = 0.05$–0.25) are given in Table 2. Outgassing of the samples before measurements was done at 300°C under vacuum ($P \cong 1.3 \times 10^{-3}$ mbar) overnight.

3.2. X-Ray Diffraction Studies

The x wt% La_2O_3/CaO samples were calcined in air at 800°C and exposed to ambient air before XRD measurements were taken. The main feature of the X-ray diffractograms was the appearance of intense diffraction peaks at 2θ positions 28.2, 34.3, and 48.9 in the case of 20 and 80 wt% La_2O_3/CaO samples. Reference to ASTM standards revealed that these peaks belong to $Ca(OH)_2$ and $La(OH)_3$ phases. Table 2 summarizes the crystal phases detected by XRD in each of the samples investigated. As it

TABLE 1

Description of Sequential Step Changes of Gas Flow during Temperature-Programmed Desorption (TPD) and Surface Reaction (TPSR) Experiments Performed over *x* wt% La_2O_3–CaO Lean-NO_x Catalysts

Experiment	Sequence of step changes of gas flow over the catalyst sample
A	0.5% NO/He (room *T*, 10 min) → He (5 min, room *T*) → TPD in He
B	0.5% NO/He (400°C, 10 min) → cool down to room *T* in NO/He flow → He (5 min, room *T*) → TPD in He
C	0.5% NO/He (room *T*, 10 min) → He (5 min, room *T*) → TPSR in 2% O_2/He
D	0.5% NO/He (room *T*, 10 min) → He (5 min, room *T*) → TPSR in 2% CH_4/He
E	0.2% NO/ 0.67% CH_4/5% O_2 (550°C, 10 min) → Cool down to 400°C in reaction mixture → He (5 min, 400°C) → TPD in He
F	Air (800°C, 1 h) → H_2 (800°C, 1 h) → He (5 min, 800°C) → cool down in He flow to room *T* → 0.5% NO/He (room *T*, 10 min) → He (5 min, room *T*) → TPD in He
G	Air (800°C, 1 h) → CH_4 (800°C, 1 h) → He (5 min, 800°C) → cool down in He flow to room *T* → 0.5% NO/He (room *T*, 10 min) → He (5 min, room *T*) → TPD in He
H	2.0% O_2/He (room *T*, 10 min) → He (5 min, room *T*) → TPD in He
I	2.0% O_2/He (550°C, 10 min) → cool down to room *T* in O_2/He flow → He (5 min, room *T*) → TPD in He
J	2% CO_2/He (room *T*, 10 min) → He (5 min, room *T*) → TPD in He
K	2% CO_2/He (room *T*, 10 min) → He (5 min, room *T*) → 0.5% NO/He (room *T*, 10 min) → He (5 min, room *T*) → TPD in He

will be discussed later, these new phases are formed due to the exposure of La_2O_3/CaO samples to ambient air. At 800°C, all these phases are absent.

3.3. Scanning Electron Microscopy (SEM) Studies

Results of the investigation on the morphology of La_2O_3/CaO mixed-oxides are as follows. In general, there was a broad distribution (0.5–1000 μm) of the particle size in all samples. By adding La_2O_3 crystallites at 50 wt% in the CaO phase, large grains with rather smooth external surface areas were formed as compared to the cases of 5 and 20 wt% La_2O_3/CaO systems. In the cases of 80 and 95 wt% La_2O_3/CaO, aggregates of undefined structure with rough edges and spongy-like surfaces to a large extent have been observed.

TABLE 2

Surface Areas and Crystalline Phases for the *x* wt% La_2O_3–CaO Systems

Composition *x* wt% La_2O_3	BET (m^2/g)[a]	Crystalline Phases (XRD Analysis)[b]
0 (CaO)	15.5	—[c]
5	11.0	CaO, La_2O_3, $CaCO_3$ (vaterite)
20	7.8	CaO, La_2O_3, $CaCO_3$ (vaterite) $Ca(OH)_2$, $La_2O_2CO_3$
50	7.5	CaO, La_2O_3, $CaCO_3$ (vaterite) $Ca(OH)_2$, $La_2O_2CO_3$, $La(OH)_3$
80	14.0	CaO, La_2O_3, $CaCO_3$ (vaterite) $La(OH)_3$
95	7.0	CaO, La_2O_3, $CaCO_3$ (vaterite) $Ca(OH)_2$, $La_2O_2CO_3$
100 (La_2O_3)	8.9	—[c]

[a] The samples were outgassed at 300°C and 1.3×10^{-3} mbar (vacuum) overnight.

[b] Following calcination at 800°C the sample had been exposed to ambient air before XRD measurements were taken.

[c] Not performed.

Catalytic Studies

Figure 2 shows intrinsic initial rates of NO consumption in terms of gram-basis (μmoles/g s, Fig. 2a) and site reactivity (TOF, s^{-1}) values (Fig. 2b) as a function of catalyst composition. Reaction conditions pertain to $T = 550$°C and a feed consisting of 0.2% NO, 0.67% CH_4, 5% O_2, and He as balance gas. The dashed curve shown in Fig. 2a corresponds to the reaction rate that would be expected over the mixture of the two phases (R_m). This rate is calculated based on the individual rates of each phase and the concentration (x, wt%) of the phase in the mixture according to

$$R_m = (x/100) \cdot R_{La2O3} + (1 - (x/100)) \cdot R_{CaO}. \quad [3]$$

If there is no cooperation (synergy) between the two phases, then the experimental rate observed over the mixture of the two solids must be predicted by Eq. [3].

As shown in Fig. 2a, there is a significant difference between the experimentally observed rate and that predicted by Eq. [3] for the 5 wt% La_2O_3/CaO sample, while this difference is reduced with increasing La_2O_3 content. In all cases, a positive synergy effect for the reaction rate is observed. It is noted that the N_2 selectivity of the present reaction was found to be higher than 95% over the whole range of catalyst composition. Some small amounts of N_2O were measured for the samples containing more than 50 wt% La_2O_3. The selectivity parameter, α, as described in a previous section, was varied between 78 and 90%, indicating that the present materials make an efficient use of CH_4 in selectively reducing the NO to N_2.

The site reactivity (TOF, s^{-1}) of the 5 wt% La_2O_3/CaO sample is found to be the highest among the 0, 5, 80, and 100 *x* wt% La_2O_3/(100 − *x*) wt% CaO solids (Fig. 2b). A site

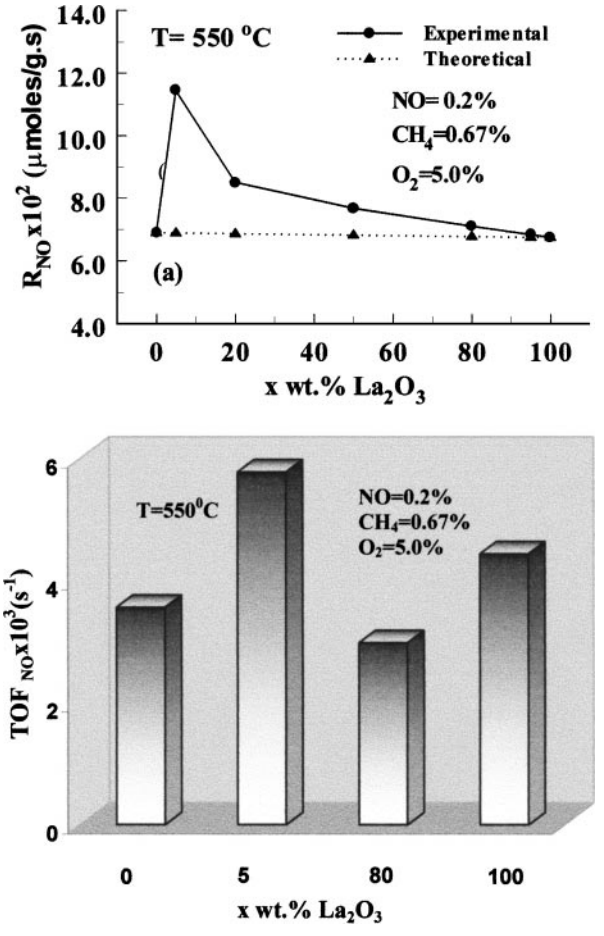

FIG. 2. Intrinsic rates of NO consumption per gram basis (a) and in terms of TOF (s^{-1}) (b) as a function of La_2O_3 content (x, wt%) in the CaO/La_2O_3 mixture obtained during $NO/CH_4/O_2$ reaction at 550°C. The solid line in (a) corresponds to experimental values, while the dashed line corresponds to the values obtained according to the mixing rule: $R_m = (x/100)\ R_{La2O3} + (100-x)/100.\ R_{CaO}$. Feed conditions: 0.2% NO, 0.67% CH_4, 5% O_2.

reactivity of 6×10^{-3} s^{-1} is calculated for the 5 wt% La_2O_3/CaO sample at 550°C and the indicated feed reaction conditions. Specific reaction rates based on BET areas (μmoles/m^2 s) are not reported since the BET areas measured do not likely correspond to the true BET values that would be obtained if the solid were treated *in situ* in air at 800°C instead of 300°C under vacuum (see Section 3.2). Catalytic and kinetic results at higher temperatures will be reported elsewhere (13).

3.4. Surface Reactivity Studies by Transient Methods

3.4.1. NO temperature-programmed desorption (TPD) following adsorption at 30 and 400°C over an air-pretreated catalyst. The chemical interaction of NO with the surface of x wt% La_2O_3/CaO solids was studied by performing adsorption of NO at 30 or 400°C followed by TPD in He flow. Before NO chemisorption was taken place, the catalyst was pretreated with air at 800°C for 2 h and purged in He at 800°C to ensure a surface "free" of carbonate species. The TPD spectra, shown in Fig. 3 with a solid line, correspond to the case of NO adsorption at 30°C (Exp. A, Table 1), while the TPD spectra with a dotted line correspond to the case of NO adsorption at 400°C followed by cooling of the sample in NO/He flow to 30°C (Exp. B, Table 1). In the case of CaO (Fig. 3A), three distinct desorption peaks are obtained in both experiments. A significant shift to lower temperatures of all three TPD peaks is observed by increasing the

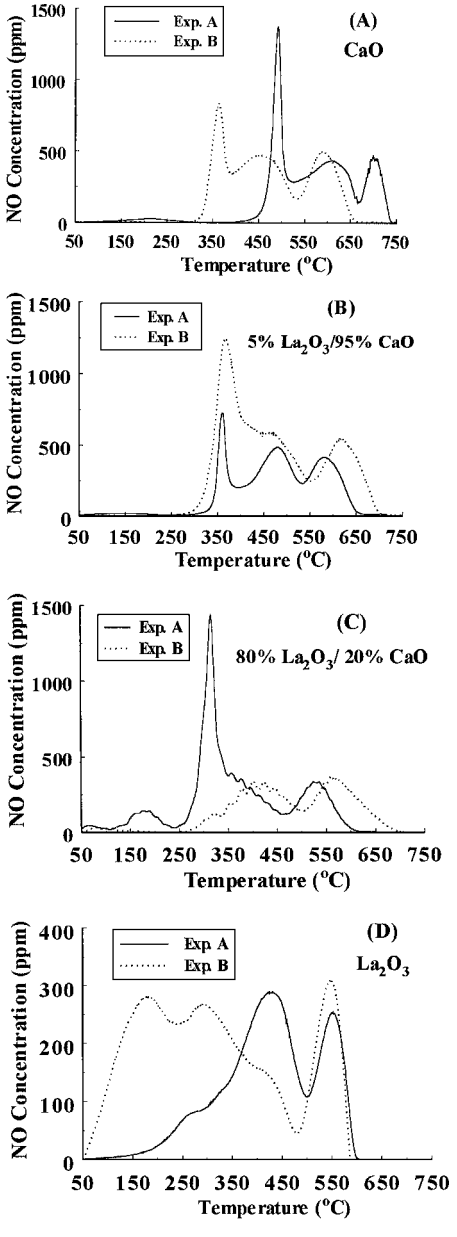

FIG. 3. Temperature-programmed desorption of NO in He flow according to Expt. A and Expt. B described in Table 1 on x wt% La_2O_3/CaO systems. (A) $x = 0$ wt%, (B) $x = 5$ wt%, (C) $x = 80$ wt%, (D) $x = 100$ wt%. $W = 0.2$ g; $q = 30$ scc/min; $\beta = 30$°C/min.

adsorption temperature from 30 to 400°C. On the other hand, the shape of the TPD spectra and the total amount of desorbed NO remain practically the same.

In the case of 5 wt% La_2O_3/CaO, the TPD spectrum obtained following NO adsorption at 30°C exhibits also three peaks as in the case of CaO but with new features. All desorption peaks shift now to lower temperatures and their relative amounts are different when compared to the case of CaO. When the temperature of adsorption was increased to 400°C, the 2nd peak (the numbering of desorption peaks follows the direction of increasing temperature) appears as a shoulder to the falling part of the 1st peak, and only the position of 3rd peak changes. In contrast, a drastic increase in the total amount of adsorbed NO is obtained (an increase by a factor of 2.5 is observed). By further increasing the content of La_2O_3 to 80 wt%, the TPD spectrum of NO is drastically altered (Fig. 3C). Most of the NO desorbs now at temperatures lower than 450°C, a result opposite to that obtained with CaO and 5 wt% La_2O_3/CaO samples. In addition, low-temperature desorption peaks ($T_M = 66$ and 177°C) and a shoulder to the falling part of the 3rd peak appear. For the adsorption temperature of 400°C, the total amount of desorbed NO decreases, a result opposite to that obtained for the 5 wt% La_2O_3/CaO, while the low-temperature desorption peaks disappear (see Fig. 3C). Small TPD peaks of O_2 (1.9 μmol/g_{cat}) and N_2 (1.75 μmol/g_{cat}) have been observed in the 450–700°C range, but not any N_2O or NO_2 peaks.

In the case of pure La_2O_3, two distinct desorption peaks and a shoulder to the rising part of the first peak are observed, following NO adsorption at 30°C (Fig. 3D). In addition, La_2O_3 is found to adsorb the least amount of NO (per gram basis) among the catalysts studied. Adsorption of NO at 400°C had the greatest effects on the NO TPD behavior as compared to the other three samples. An interesting result is the large amount of NO desorbed in the low-temperature range of 50–250°C. By contrast to the case of 80 wt% La_2O_3/CaO, adsorption of NO at 400°C on La_2O_3 resulted in a significant increase of NO uptake as compared to that obtained following adsorption at 30°C. The total amount of adsorbed NO and all peak maximum positions observed in the TPDs of Fig. 3 are given in Table 3. From the results of Table 3 it is concluded that NO chemisorption on the 5 and 80 wt% La_2O_3/CaO samples does not follow the mixing rule (similar to Eq. [3]).

3.4.2. O_2 TPDs following adsorption at 30 and 550°C over an air-pretreated catalyst. The chemical interaction of O_2 with the surface of the present catalysts was studied in a similar manner as in the case of NO (see Expts. H and I, Table 1). Figure 4 reports O_2 TPD response curves as a function of catalyst composition and adsorption procedure. In the case of pure CaO and 5 wt% La_2O_3/CaO systems, the O_2 TPD spectra are similar in position ($T_M = 597$°C) and shape. The only difference is the larger amount of O_2 uptake obtained with the 5 wt% La_2O_3/CaO during the high-temperature adsorption step as compared to the pure CaO. The amount of O_2 chemisorption as a function of catalyst composition and adsorption procedure is presented in Fig. 5. By increasing the La_2O_3 content to 80 wt%, significant alterations to the O_2 TPD response curves are observed. In the case of adsorption at 30°C, the peak shifts to higher temperatures ($T_M = 603$°C), while in the case of adsorption at 400°C the oxygen desorbs at lower temperatures ($T_M = 525$°C). In contrast, the amount of O_2 uptake is now lower than that obtained on CaO and 5 wt% La_2O_3/CaO samples (see Fig. 5). For pure La_2O_3, the O_2 TPD spectra shift to lower temperatures and two peaks are now seen for the case of adsorption at 550°C (Fig. 4D, curve b). On the other hand, La_2O_3 gives the lowest amount of O_2 adsorption at both adsorption temperatures with respect to the other three catalysts.

TABLE 3

Amount (μmol/g_{cat}) and Peak Maximum Temperatures (T_M) of NO Desorbed during Temperature-Programmed Desorption (TPD) Experiments over x wt% La_2O_3–CaO Lean-NO_x Catalysts

Catalyst x wt% La_2O_3	Total amount of desorbed NO (μmol/g_{cat})	T_M (°C)
0 (CaO)	19.4[a]	216,[a] 493, 611, 701
	21.6[b]	364,[b] 455, 590
5	19.8[a]	361,[a] 480, 583
	50.5[b]	367,[b] 615 shoulder (430–490)
80	23.9[a]	66,[a] 177, 316, 525
	16.1[b]	305,[b] 537 shoulder (320–420)
100 (La_2O_3)	12.4[a]	424,[a] 554 shoulder (230–280)
	25.4[b]	175,[b] 292, 548 shoulder (380–430)

[a] Values correspond to NO adsorption at room temperature (Expt. A).
[b] Values correspond to NO adsorption at 400°C (Expt. B).

3.4.3. CO_2 TPDs following adsorption at 30°C over an air-pretreated catalyst. The x wt% La_2O_3/CaO catalysts have shown significant differences in their catalytic activity toward NO/CH_4/O_2 reaction (Fig. 2 and Ref. (13)). Under integral reactor conditions (high CH_4 conversions) the concentration of CO_2 produced was significant (13). It is known that under practical lean-NO_x conditions the concentration of CO_2 in the exhaust gas is in excess of 8–10 mol%. It is, therefore, important to study the chemisorptive behavior of CO_2 with the La_2O_3/CaO catalysts in order to obtain information that might be related to the catalytic results obtained. For this, CO_2 adsorption experiments followed by TPD in He flow have been conducted (see Expt. J, Table 1) and the results obtained are shown in Fig. 6. An important feature is the monotonic shift of the position of the CO_2 TPD response curve to lower temperatures by increasing the wt% content of La_2O_3 in the La_2O_3/CaO

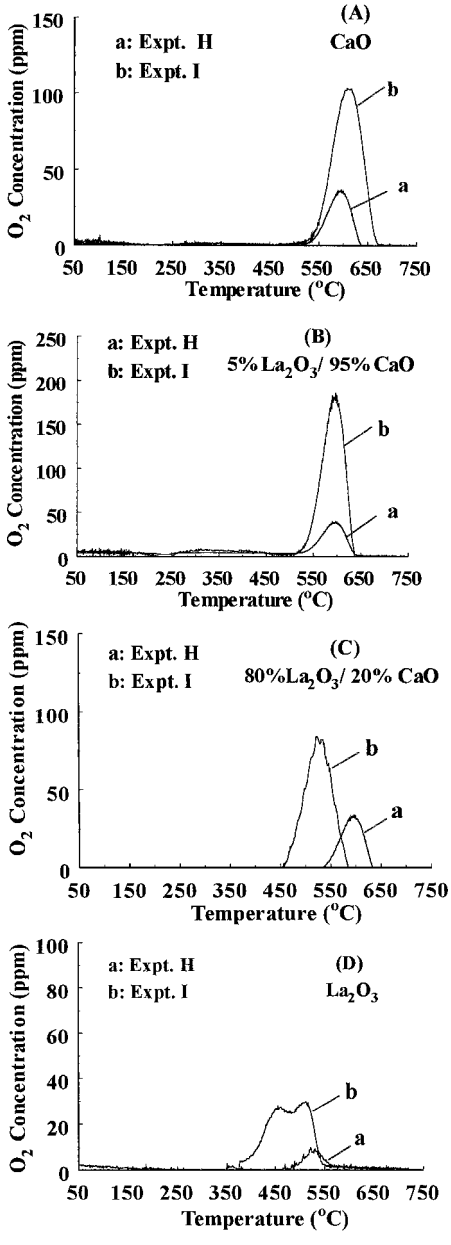

FIG. 4. Temperature-programmed desorption of O_2 in He flow according to Expt. H and Expt. I (Table 1) on x wt% La_2O_3/CaO systems. (A) $x = 0$ wt%, (B) $x = 5$ wt%, (C) $x = 80$ wt%, (D) $x = 100$ wt%. $W = 0.2$ g; $q = 30$ scc/min; $\beta = 30°$C/min.

system. On the other hand, increasing the La_2O_3 content from 0 to 5 wt% results in an increase of about 30% in the uptake of CO_2 (136.7 vs 172.5 μmol/g_{cat}), while a further increase to 80 wt% La_2O_3 results in a drastic decrease in the CO_2 uptake (40 μmol/g_{cat}). Over pure La_2O_3 the CO_2 chemisorption was found to be 56.2 μmol/g_{cat}.

3.4.4. NO and CO_2 TPDs after adsorption of CO_2 followed by NO adsorption at 30°C over an air-pretreated catalyst. The interaction of NO with preadsorbed CO_2 was

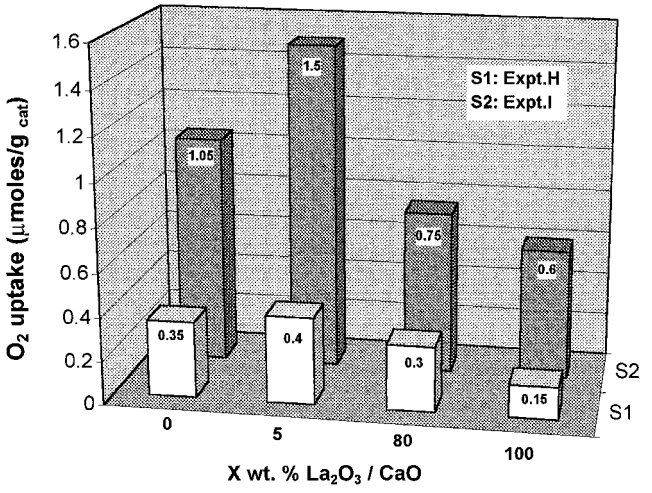

FIG. 5. Oxygen uptakes (μmoles/g_{cat}) determined by the experimental procedures according to Expt. H and Expt. I (Table 1) as a function of catalyst composition (x wt% La_2O_3/CaO).

studied as follows. A 2 mol% CO_2/He mixture was first passed over the catalyst surface at room temperature for 10 min. The feed was then switched to pure He for 5 min and then to a 0.5 mol% NO/He mixture for 10 min, followed by a 5-min He purge and a TPD (see Expt. K, Table 1). Figure 7 presents the NO and CO_2 TPD response curves obtained as a function of catalyst composition. A comparison of the CO_2 response curves of Figs. 6 and 7 clearly indicates that the shape of these curves for all catalyst formulations has changed only slightly. On the other hand, the amount of CO_2 desorbed is found to be lower than that observed in Fig. 6, except in the case of 80 wt% La_2O_3/CaO sample. This behavior is illustrated in Fig. 8 via the parameter S_2 (the ratio of desorbed amount of CO_2 for Expt. J to that for Expt. K). A similar behavior is also observed in the case of desorbed NO shown in Fig. 7 and that shown in

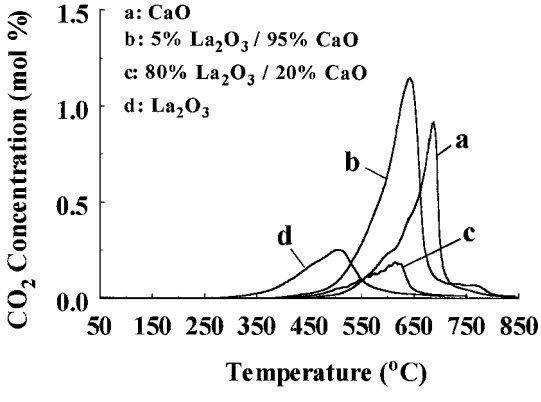

FIG. 6. Temperature-programmed desorption of CO_2 in He flow according to Expt. J (Table 1) on x wt% La_2O_3/CaO systems. (a) $x = 0$ wt%, (b) $x = 5$ wt%, (c) $x = 80$ wt%, (d) $x = 100$ wt%. $W = 0.2$ g; $q = 30$ scc/min; $\beta = 30°$C/min.

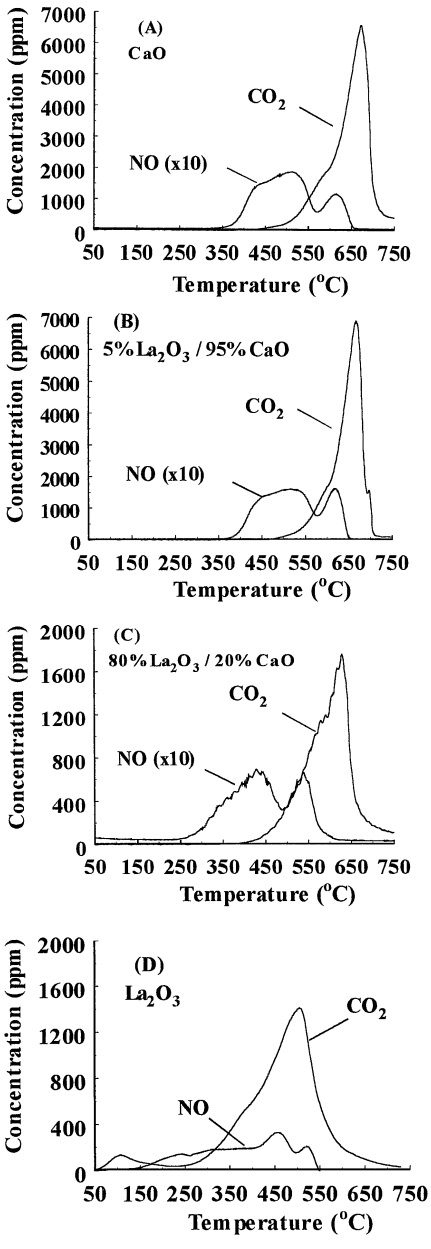

FIG. 7. Temperature-programmed desorption of NO and CO_2 in He flow according to Expt. K (Table 1) on x wt% La_2O_3/CaO systems. (A) $x = 0$ wt%, (B) $x = 5$ wt%, (C) $x = 80$ wt%, (D) $x = 100$ wt%. $W = 0.2$ g; $q = 30$ scc/min; $\beta = 30°$C/min.

Fig. 3 (Expt. A) and is illustrated in Fig. 8 via the parameter S_1 (the ratio of desorbed amount of NO for Expt. A to that for Expt. K). Thus, preadsorbed CO_2 causes a drastic decrease in the uptake of NO and it also affects significantly the kinetics of NO desorption (compare Figs. 3 and 7).

3.4.5. NO TPDs following adsorption at 30°C over H_2- and CH_4-pretreated catalyst. The interaction of NO with the surface of x wt% La_2O_3/CaO system pretreated with either CH_4 or H_2 was also studied. Methane is one of the reactants for the present reaction system, while hydrogen might be an intermediate product of the $CH_4/NO/O_2$ reaction for the present catalytic surfaces. Hydrogen is produced over these materials under CH_4/O_2 reaction conditions similar to the ones of the present work (16).

Figure 9 presents TPD of NO response curves after the catalyst was pretreated with H_2 (Expt. F) or CH_4 (Expt. G) at 800°C for 1 h. For comparison purposes, the TPD of NO response obtained after the surface was pretreated with air is also given (Expt. A). The NO TPD response curves (Expt. F and G) appear to have been altered significantly in shape, position and amount of NO adsorption as compared to the case of the air-pretreated catalyst. In the case of CaO, there is a decrease by about 25% in the amount of NO adsorption for both H_2- and CH_4-pretreated surfaces, while in the case of La_2O_3 no change in the total amount of NO chemisorption has been observed. However, in the case of lanthana the effect of CH_4-pretreatment is to increase the amount of desorbed NO at low temperatures (see Fig. 9D). In the case of 5 wt% La_2O_3/CaO pretreatment of the catalyst with H_2 has the effect of increasing the amount of NO adsorption by a factor of 1.6, while in the case of CH_4 by a factor of 2.1. On the other hand, by increasing the content of La_2O_3 to 80 wt% results in a larger decrease of the amount of NO adsorption than that observed on pure CaO. All the quantitative results of Fig. 9 are given in Table 4.

3.5. Temperature-Programmed Surface Reaction (TPSR) Studies

3.5.1. TPSR with CH_4/He flow. The reactivity of preadsorbed NO on the La_2O_3/CaO surface toward CH_4 was studied by the TPSR technique. Following adsorption of

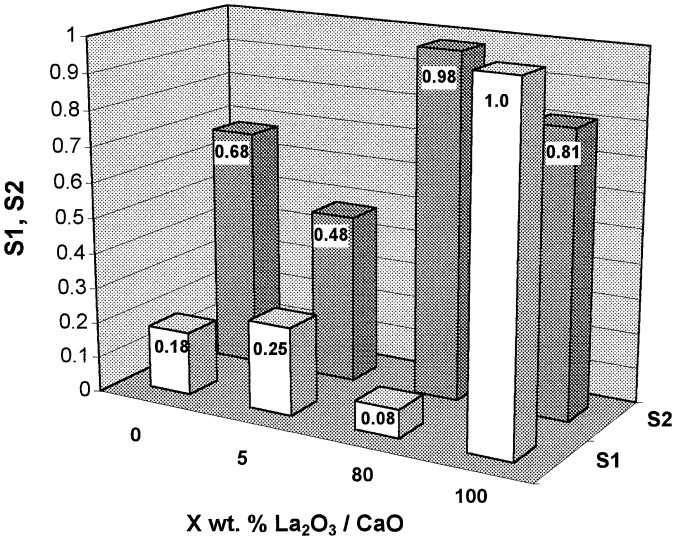

FIG. 8. Ratio (S_1) of the amount of NO desorbed in Expt. K to that in Expt. A, and ratio (S_2) of the amount of CO_2 desorbed in Expt. K to that in Expt. J as a function of x wt% La_2O_3/CaO catalyst composition.

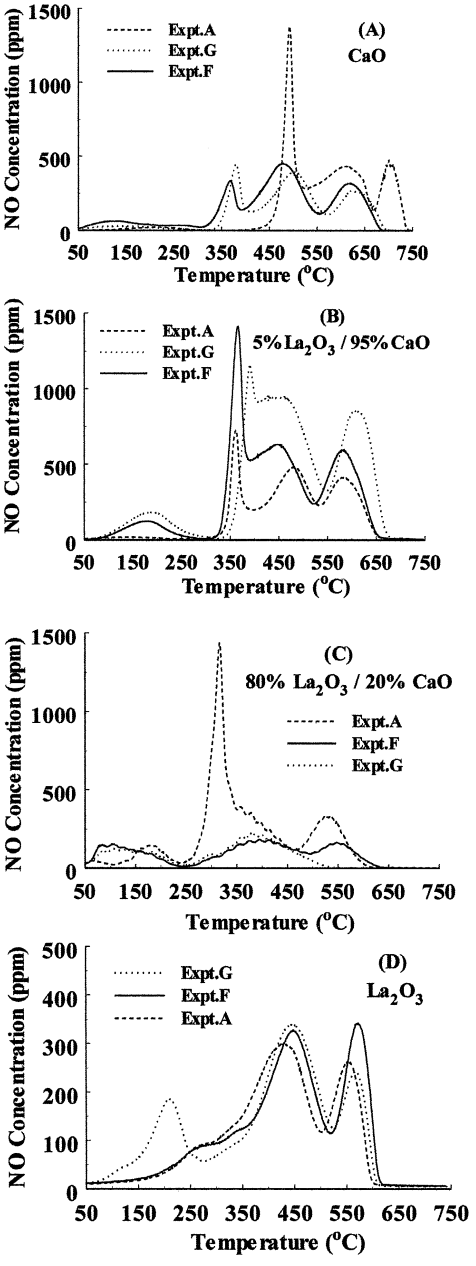

FIG. 9. Temperature-programmed desorption of NO in He flow following adsorption at room temperature for a sample pretreated with H_2 (curve a), CH_4 (curve b), and air (curve c) according to Expt. F, Expt. G, and Expt. A (Table 1), respectively. (A) CaO, (B) 5 wt% La_2O_3/CaO, (C) 80 wt% La_2O_3/CaO, (D) La_2O_3. $W = 0.2$ g; $q = 30$ scc/min; $\beta = 30°$C/min.

NO at 30°C over a surface that had been pretreated with air at 800°C and purged in He, the feed was changed to a 2% CH_4/He mixture. The temperature of the catalyst was then increased to 800°C at the rate of 30°C/min (see Expt. D, Table 1). Figure 10 presents the NO response curves obtained as a function of catalyst composition. It is noted that neither N_2O nor NO_2 was observed in the 50–750°C range. Only small amounts of CO_2 were observed at $T > 750$°C

TABLE 4

Amount of NO Desorbed (μmol/g_{cat}) during Various Kinds of Temperature-Programmed Desorption (TPD) and Surface Reaction (TPSR) Experiments under Different Gas Atmospheres over *x* wt% La_2O_3–CaO Lean NO_x Catalysts

Experiment Code (see Table 1)	*x* wt% La_2O_3–CaO			
	0 (CaO)	5	80	100 (La_2O_3)
C	16.8	18.3	24.6	6.15
D	17.6	18.3	21.5	11.9
E	7.1	9.3	5.9	7.3
F	15.8	32.5	9.7	12.3
G	13.5	42.2	11.7	12.8

due to reaction of methane with the surface lattice oxygen of the catalyst. In addition, very small amounts of N_2 (<10 ppm) but not any O_2 were observed in the 550–650°C range due to reaction of adsorbed NO with CH_4.

A comparison of the NO response curve shown in Fig. 10 for a given catalyst formulation with the corresponding curve shown in Fig. 3 indicates the drastic changes that occurred in the desorption kinetics of NO in the presence of gaseous CH_4. In all catalysts except of CaO the amount of NO desorbed in the 50–300°C range increases significantly. In general, desorption peak positions and their relative amounts have been extensively influenced by the presence of CH_4. The total amount of desorbed NO obtained is given in Table 4. This amount is found to be less by 5–10% than the amount measured after TPD in He flow (Expt. A vs Expt. D). This difference is due to the small extent of NO reduction by CH_4 at the higher temperatures.

3.5.2. TPSR with O_2/He flow. Figure 11A presents NO transient response curves obtained after a TPSR experiment with 2% O_2/He flow had been performed (see

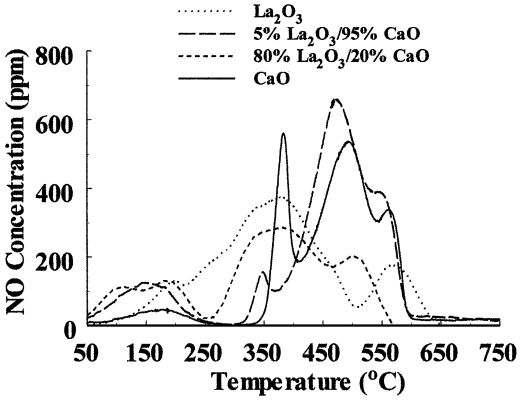

FIG. 10. Transient NO response curves observed during temperature-programmed surface reaction (TPSR) in CH_4/He flow of preadsorbed NO according to the sequence given in Expt. D (Table 1) on *x* wt% La_2O_3/CaO systems. $W = 0.2$ g; $q = 30$ scc/min; $\beta = 30°$C/min.

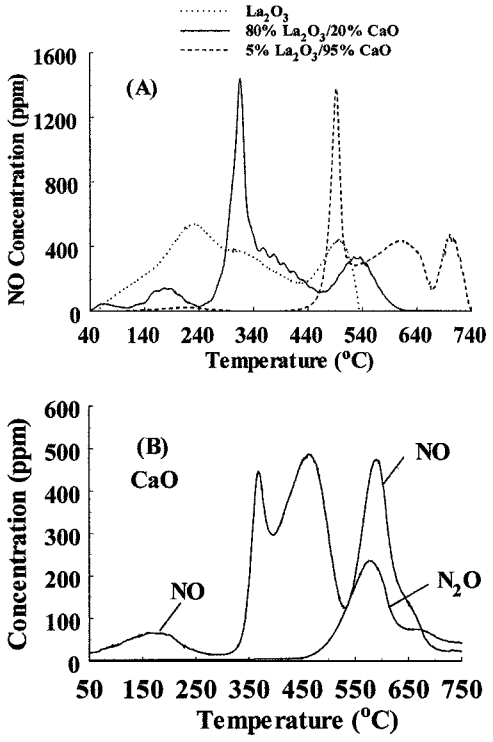

FIG. 11. (A) Transient NO response curves observed during temperature-programmed surface reaction (TPSR) in O_2/He flow of preadsorbed NO according to the sequence given in Expt. C (Table 1) on x wt% La_2O_3/CaO systems. (B) Transient NO and N_2O responses observed during temperature-programmed surface reaction (TPSR) in O_2/He flow of preadsorbed NO according to the sequence given in Expt. C (Table 1) on CaO. $W = 0.2$ g; $q = 30$ scc/min; $\beta = 30°$C/min.

Expt. C in Table 1) on x wt% La_2O_3/$(100 - x)$ wt% CaO samples ($x = 5$, 80, and 100). Figure 11B presents the transient response curves of NO and N_2O obtained on CaO for the same TPSR experiment. Drastic changes in the NO desorption spectra of Fig. 11 occurred when these spectra are compared to the curves observed in He flow (Fig. 3). In the case of CaO (Fig. 11B), the presence of O_2 causes the NO to desorb at lower temperatures as compared to the case of pure He. In addition, the amount of NO that corresponds to a given desorption peak changes significantly (compare Figs. 3A and 11B). The amount of NO desorbed during TPSR in O_2/He flow is given in Table 4.

3.6. *Transient Isothermal Desorption of NO Followed by TPD*

The measurement of NO chemisorption under NO/CH_4/O_2/He reaction conditions was performed as follows. After reaction at 550°C for 10 min, the sample was quickly cooled to 400°C under the reaction mixture. The feed was then switched to He for 5 min, while at the same time the NO signal was recorded by on-line mass spectrometry. After the NO signal reached the background value in He flow, the temperature was increased to 800°C to carry out a TPD run. The amount of NO desorbed isothermally at 400°C was found to be 0.9 μmol/g_{cat}, while that under the TPD run was 6.4 μmol/g_{cat} (desorbed in the 420–620°C range, $T_M = 530$°C). Table 4 reports the total amount of NO chemisorption for this experiment as a function of catalyst composition. It is observed that the 5 wt% La_2O_3/CaO sample adsorbs the largest amount of NO, while the amount of NO adsorbed under reaction conditions is significantly lower than the amount adsorbed at 30°C from the NO/He gas mixture.

3.7. *Effects of Carrier Gas Composition on the NO TPD Response Curves*

Theoretical and experimental studies have demonstrated that in a TPD experiment the carrier gas composition can influence both the peak maximum temperature (T_M) and the maximum desorption rate (17). To check the possibility whether the drastic changes in the position and shape of the NO response curves observed in the TPSR experiments of Figs. 10 and 11 might be due to external mass transfer effects, NO TPD experiments with Ar as a carrier gas were conducted. The TPD response curves of NO obtained on La_2O_3 when Ar or He carrier gas was used had indicated no change in the position of the high-tempeature desorption peak of NO but only a small shift of the 1st NO TPD peak (Fig. 3D) to lower temperatures. In addition, very small differences appeared in the shape of the TPD curves for the two carrier gases used.

4. DISCUSSION

4.1. *NO Chemisorption Followed by TPD*

A few infrared studies of NO adsorption at room or higher temperatures on CaO (18, 19) and La_2O_3 (20–22) have been performed. Other infrared works focused on the kinds of adsorbed NO species that truly participate in the decomposition reaction of NO (19, 22–26). In the infrared studies on CaO and La_2O_3 surfaces (19, 22) the adsorbed NO species identified are listed in Scheme 1. There are six different structures of adsorbed NO each of which is characterized by its own thermal stability. Scheme 1 presents also the various reaction paths for the formation of adsorbed NO species in accordance to the literature (19, 22). Based on Scheme 1, it is reasonable to suggest that the three distinct NO TPD peaks obtained with CaO and the four peaks with La_2O_3 is likely to correspond to different structures of adsorbed NO species. However, one cannot exclude the possibility that the same structure may also exist on different sites. Such heterogeneity is expected to exist on metal oxide surfaces (27).

In the infrared work of NO adsorption on CaO (19), it was suggested that isomerization of nitro to nitrito species

is likely to occur and this process is considered to be an activated process. In the case of MgO (28), it has been observed that the mononitrosyl species reached their maximum intensities within a much shorter period of time than the intensities of the dinitrosyl species ($N_2O_2^{2-}$). It was suggested (28) that the latter species can interact with other adsorbed NO species according to the reaction

$$N_2O_2^{2-} + NO_2^- \rightarrow 2NO(g) + NO^- + O^{2-}. \qquad [4]$$

Based on what was mentioned in the previous paragraph, the following can be offered to explain the TPD of NO behavior observed on CaO (Fig. 3A). By increasing the adsorption temperature to 400°C some conversion of nitro to nitrito species (an activated process) and of NO_2^- to NO^- species according to reaction [4] is likely to have occurred. Desorption of nitrito and NO^- species is then expected to occur at lower temperatures than of NO_2^- or NO_2^{2-} species (see Scheme 1).

The high NO adsorption temperature of 400°C used for La_2O_3 caused a significant population of adsorbed NO species with low binding energies (Fig. 3D). In addition, the amount of adsorption is found to be twice that obtained following adsorption at 30°C, a behavior opposite to that observed on CaO. On the other hand, the NO desorption peak with the highest peak maximum temperature remains practically the same in position and amount. These results suggest that La_2O_3 pocesses a significant fraction of activated sites for NO chemisorption. Klingenberg and Vannice (26) have found that formation of anionic NO^- species is promoted by the defect structure of lanthana. These species are responsible for the formation of $N_2O_2^{2-}$ species. It is, therefore, likely that the large increase of NO adsorption observed on La_2O_3 during adsorption at 400°C is associated with the formation of $N_2O_2^{2-}$ and/or $N_2O_2^-$ species. Since decomposition of NO at 400°C had not been observed on the present La_2O_3, the explanation that the TPD behavior of Fig. 3D could be due to some modification of the La_2O_3 surface that occurred during adsorption at 400°C must be excluded.

Of great importance are the TPD of NO results observed for the 5 wt% (Fig. 3B) and 80 wt% La_2O_3/CaO (Fig. 3C) samples with respect to their catalytic activity behavior (Fig. 2). The former catalyst exhibits three times higher specific uptake of NO, it has the largest amount of NO adsorption under reaction conditions and the largest amount of desorbed NO at $T > 550$°C with respect to the latter catalyst. These results can be used to partly explain the highest intrinsic activity exhibited by the 5 wt% La_2O_3/CaO sample (Fig. 2) among the series of solids investigated.

The TPD results of NO shown in Figs. 3B and 3C suggest also that new catalytic sites were created upon wet mixing of the two oxide phases followed by air calcination at 800°C. It is noted that both catalytic systems exhibit large deviations from the mixing rule (Eq. 3) with respect to NO chemisorption. It has been reported (29) that Ca^{2+} ions can favorably be incorporated into the crystal lattice of lanthana (dopant substitution) resulting in the creation of oxygen vacancies for charge compensation. It has also been reported that doping of a metal oxide can largely influence the chemisorptive properties of its surface (30). A similar doping procedure of CaO by La^{3+} is also possible (30). Klingenberg and Vannice (22) pointed out the importance of oxygen vacancies toward the formation of NO^- and $N_2O_2^{2-}$ species on the lanthana surface. These results along with the photoluminescence studies (13) on the present catalysts that probed the existence of oxygen vacancies could be used to explain the observed chemisorption behavior of NO on the 5 wt% La_2O_3/CaO system. The SEM results could also be used to support the presence of different catalytic sites over the 5 and 80 wt% La_2O_3/CaO systems due to the observed differences in their particle morphology. TEM studies reported by Lacombe *et al.* (31) have shown that various kinds of local surface defects can be developed with lanthana particles (e.g., grain boundaries of high tension, crystalline microareas with different plane orientations, and regular steps). As it will be discussed in the next section, the present XRD results do not support the formation of new crystal phases for the La_2O_3/CaO system after being calcined at 800°C and kept under inert atmosphere.

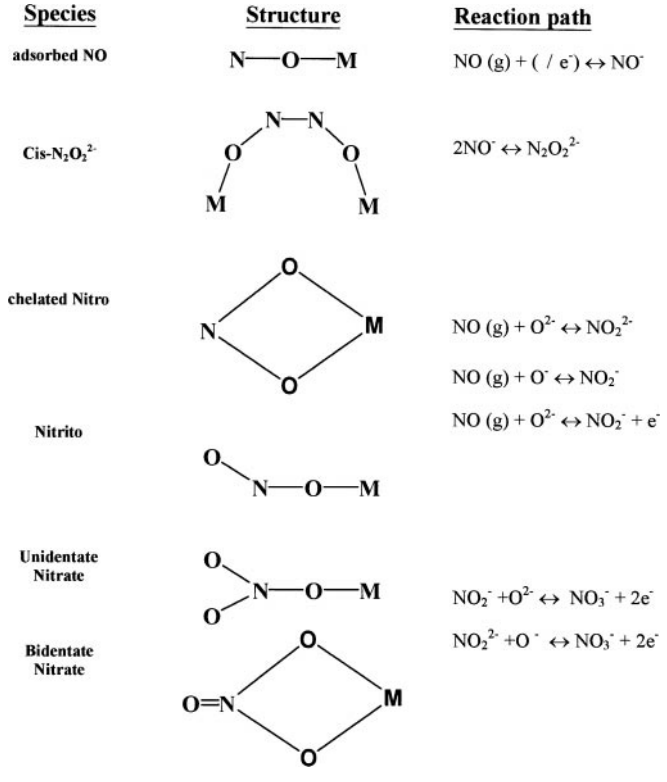

SCHEME 1. Various adsorbed NO structures and the reaction path of their formation on CaO and La_2O_3 surfaces.

4.2. CO_2 Chemisorption. Effects of Preadsorbed CO_2 on the Adsorption/Desorption Kinetics of NO

Infrared studies (32) have shown that decomposition of $Ca(OH)_2$ to the oxide form is complete at 800°C. Similarly, the decomposition of $CaCO_3$ to CaO is complete at 800°C (33). Lanthanum oxide is known to be very sensitive to water and carbon dioxide (34), and its exposure to ambient air leads to bulk hydroxylation and carbonation. The hydroxyl compounds thus formed are readily decomposed by heating to 300°C (35), while the carbonate phases are decomposed at higher temperatures in the 650–800°C range (31, 34, 36). In a recent study (21) it was found that small amounts of carbonates could persist on lanthana surfaces at temperatures higher than 800°C. Based on these observations, it is concluded that the new crystal phases reported in Table 2 can not be expected to be present at 800°C. Only small amounts of surface carbonates may be considered to resist on the present surfaces.

The TPDs of CO_2 correspond therefore to adsorption on the pure phases of CaO and La_2O_3 and on new sites formed in the CaO/La_2O_3 mixed oxide system. The results of Fig. 6 clearly indicate that the surface of CaO exhibits the highest bond strength with adsorbed CO_2, while the La_2O_3 surface exhibits the lowest bond strength among the catalysts investigated. When 5 wt% of La_2O_3 is added to the CaO sample a significant change in the amount and bond strength of CO_2 adsorption is obtained compared to the case of CaO. While pure La_2O_3 adsorbs the least amount of CO_2 among the four samples, the 5 wt% La_2O_3/CaO adsorbs the largest amount. These results again strongly suggest that new catalytic sites have been formed during the preparation and calcination procedures applied for the solids investigated.

A recent infrared work (21) revealed that adsorption of CO_2 at room temperature over lanthana leads initially to the formation of bidentate carbonates which then are converted into unidentate species during heating to 500°C. Adsorption of CO_2 at 500°C produces only the unidentate carbonate species (21). The shape of the CO_2 TPD peak observed on La_2O_3 and 80 wt% La_2O_3/CaO samples (Fig. 6) confirms the infrared results of Klingenberg and Vannice (21). Yang *et al.* (37) have performed CO_2 TPD studies on CaO, La_2O_3, and 10 wt% La_2O_3/CaO samples. The order of increase of the T_M value for the three samples agrees with that found here (Fig. 6).

By comparing the TPD spectra shown in Figs. 3, 6, and 7, it is concluded that preadsorbed CO_2 on La_2O_3/CaO caused drastic changes in the desorption kinetics of NO. A striking result is the significant decrease of the amount of desorbed CO_2 when NO had been adsorbed onto the catalyst surface following CO_2 chemisorption (see Fig. 8, S_2). This important result requires some explanations. A hypothesis was made that during adsorption of NO at room temperature, following CO_2 chemisorption, some desorption of CO_2 might have been taken place and, therefore, the CO_2 amount measured by TPD was expected to be lower. To check this hypothesis, at the end of the CO_2 adsorption step the gas flow to the reactor was changed to 0.5% NO/He for 5 min and the reactor was batched for 20 min. Then, the reactor was opened to the He flow and the exit stream of the reactor was analyzed by mass spectrometry. A significant signal at $m/z = 44$, apparently from CO_2, was observed.

Klingenberg and Vannice (22) have reported the formation of gaseous CO_2 upon adsorption of NO at room temperature, upon heating of preadsorbed NO from 25 to 500°C and upon adsorption of NO at 500°C on La_2O_3. These interesting results, similar to the ones observed in the present work (Figs. 7 and 8) were interpreted based on the surface elementary reaction step

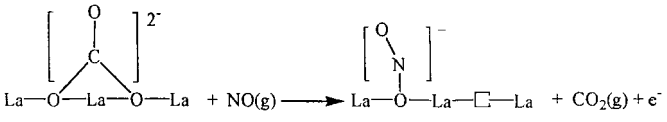

The above reaction step indicates the generation of an F center (oxygen vacancy with a trapped electron), an active site for the formation of adsorbed NO^- that produces the *cis*-$N_2O_2^{2-}$ species, the latter being responsible for the formation of N_2 during the NO decomposition reaction. The NO and CO_2 TPD results presented for La_2O_3 (Fig. 7D), when compared to those presented in Figs. 3D and 6d strongly suggest that surface reactions between adsorbed NO and carbonate species occur. The present work strongly supports the infrared results obtained by Klingenberg and Vannice (22) and the above proposed reaction step. The 5 wt% La_2O_3/CaO system has shown the largest exchange ability between adsorbed carbonate and NO species, while the 80 wt% La_2O_3/CaO system the lowest ability. In addition, the latter catalyst adsorbs the least amount of NO when CO_2 is first adsorbed on the surface. These observations can be used to explain in part the better catalytic performance exhibited by the 5 wt% La_2O_3/CaO solid (Fig. 2). It is expected that the rate of accumulation of carbonate species under lean-NO_x conditions will be lower on 5 wt% La_2O_3/CaO than on the other samples investigated. This is because a higher rate for an exchange between adsorbed NO and carbonate species that leads to the creation of sites for further NO adsorption and reduction is expected. This is an important conclusion of this work that could lead to a better design of lean-NO_x catalysts.

4.3. O_2 Chemisorption Followed by TPD

Zhang *et al.* (30) have reported O_2 TPD spectra obtained on 10 mol% CaO/La_2O_3 catalysts. The broad O_2 TPD spectra obtained in the 50–600°C range were deconvoluted into four peaks, most of the O_2 desorbed at temperatures lower

than 350°C and the strongly bound oxygen species desorbed at $T_M = 445$°C. The authors have suggested that, due to the highly mobile oxygen defects present in the CaO/La_2O_3 system, weakly adsorbed oxygen (e.g., O_2^-) can be transformed into strongly bound oxygen species (e.g., O^{2-} or O^-).

Yang *et al.* (37) have studied by the EPR technique the nature of adsorbed oxygen species on a 10 wt% La_2O_3/CaO sample calcined at 780°C. Adsorption of O_2 at room temperature over an outgassed sample resulted in the formation of O_2^- superoxide species. Following adsorption at 780°C for 1/2 h and cooling to room temperature the O_2^- EPR signal was much stronger than that obtained by O_2 adsorption at room temperature. These results suggest that O_2^- species which can also be formed at high temperatures is not transformed during cooling. The O_2^- species has also been observed on pure CaO and La_2O_3 samples but with a lower coverage than on the 10 wt% La_2O_3/CaO sample (37). The authors explained these results by stating that La_2O_3 promotes the creation of oxygen vacancies in the CaO, thus increasing the O_2^- surface concentration.

The present O_2 TPD results are significantly different than those reported by Zhang *et al.* (30) in that only high temperature desorption of O_2 is seen on the present *x* wt% La_2O_3/CaO samples. In the case of pure CaO and 5 wt% La_2O_3/CaO, the effect of adsorption temperature is in harmony with what has been reported (37) and described in the previous paragraph. An increase in the amount of lanthana to 80 wt% in the mixed oxide system results in a decrease of the binding energy of adsorbed oxygen (compare curve b in Figs. 4A–4C). This result may suggest that adsorbed oxygen (e.g., O_2^-) formed at 550°C is transformed to other oxygen species (e.g., O^- and O^{2-}) as also suggested (30). In the case of La_2O_3, adsorption of O_2 at 550°C followed by cooling to room temperature results in two kinds of adsorbed species. This result is different than that reported by Imai *et al.* (38). The amount of O_2 adsorption at 550°C is found to be four times higher than that observed after adsorption at room temperature, a result similar to that reported by Zhang *et al.* (4).

The present O_2 TPD results strongly suggest that the addition of La_2O_3 crystallites to CaO crystallites causes the creation of new sites for oxygen adsorption in addition to those present in the two pure oxide phases. These sites are suggested to be oxygen vacancies based on photoluminescence studies performed on the present samples (13). Therefore, the O_2 TPD results along with those of NO TPD strongly suggest that doping of CaO by La^{3+} and/or La_2O_3 by Ca^{2+} (creation of oxygen vacancies) has taken place. The O_2 TPD results could be related to the present catalytic activity of the La_2O_3/CaO solids (Fig. 2) since the 5 wt% La_2O_3/CaO exhibits the highest amount (per gram basis) of O_2 adsorption at 550°C, it is characterized by the largest binding energy and at the same time it shows the highest intrinsic catalytic activity (Fig. 2).

4.4. Synergistic Effects in Explaining Catalytic Activity

Photoluminescence studies (13) performed on the present series of solids revealed that the intensity of the emitted light (at $\lambda_{ex} = 200$ nm) due to the presence of F centers follows exactly the same trend as the uptake of oxygen chemisorption (Fig. 5). The relationship between the oxygen vacancies and the chemisorptive and catalytic behavior of the present solids seems to be of primary importance. As already mentioned in a previous section, doping of La_2O_3 by Ca^{2+} ions can lead to the creation of oxygen vacancies (29) and the extent of diffusion of Ca^{2+} ions into the lanthana lattice at 800°C is expected to be favored under high CaO/La_2O_3 ratios.

Based on what was mentioned in the previous paragraph and the transient reactivity results of this work, the positive synergistic catalytic effect presented in Fig. 2 must reasonably be associated with the presence of oxygen vacancies in the La_2O_3/CaO system. These new catalytic sites favor (a) adsorption of NO and its reactivity during lean-NO_x reaction conditions and (b) exchange between adsorbed CO_2 and NO that can lead to increased reaction rates and lower catalyst deactivation by CO_2 poisoning. The electronic properties of a solid surface can be influenced by doping (30), and therefore the chemisorptive and catalytic properties of the surface. In the present work, it is unknown what other surface reaction steps might have been influenced by doping. The overall superior catalytic performance of the 5 wt% La_2O_3/CaO sample with respect to the other ones (Fig. 2) may also be due to some influence of oxygen vacancies on other catalytic steps of the reaction mechanism.

Shi *et al.* (9) in their recent detailed study of $NO/CH_4/O_2$ reaction on La_2O_3 supported on Al_2O_3 catalysts reported a specific reaction rate of 0.3 μmoles $N_2/s\,g_{cat}$ at 550°C over the best catalyst composition found. In the present work, at 550°C a value of 0.057 μmoles $N_2/s\,g_{cat}$ is obtained. However, the feed reaction conditions used in the two works are quite different. Shi *et al.* (9) have used a feed containing 1.8% NO, 0.45% CH_4, and 1% O_2 to be compared to the feed of 0.2% NO, 0.67% CH_4, and 5% O_2 used here. Given the fact that over the catalyst formulations studied by Shi *et al.* (9) the reaction order with respect to NO is in the range of 0.7–0.9, while a negative order in O_2 was found (5, 11), it can be stated that the activity per gram basis of the present 5 wt% La_2O_3/CaO system is at least practically the same as that reported for the 40 wt% La_2O_3/Al_2O_3 system. In terms of site reactivity, a TOF value of 6×10^{-3} s^{-1} at 550°C for the reaction conditions shown in Fig. 2b is calculated for the 5 wt% La_2O_3/CaO system. This value was based on the irreversible amount of NO adsorption (see Expt. B). A value of 5×10^{-3} s^{-1} at 550°C is calculated for the 40 wt% La_2O_3/Al_2O_3 system (9). Considering the differences in the feed stream used in the two works and what was mentioned

TABLE 5

Comparison of Rates of NO Reduction by CH_4 in the Presence of O_2 on Different Catalysts

Catalyst	Reaction conditions					R_{N2} (μmol/s g_{cat}) $\times 10^2$	Ref.
	NO (%)	CH_4 (%)	O_2 (%)	GHSV (h^{-1})	T (°C)		
4% Li/MgO	2.02	0.5	1.0	3000	550	0.661	(6)
La_2O_3	2.02	0.5	1.0	8700	500	2.9	(5)
La_2O_3	0.082	0.082	0.5	8700	500	0.84	(5)
Co/ZSM-5	0.164	0.1025	2.5	30000	500	4.58	(42)
Y_2O_3	0.4	0.4	4.0	60000	550	16.6	(11)
40% La_2O_3/ Al_2O_3	1.8	0.45	1.0	100000	550	30.0	(9)
5% La_2O_3/ CaO	0.2	0.67	5.0	20000	550	5.9	This study
CaO	0.2	0.67	5.0	20000	550	3.5	This study

above with respect to this point, it can be concluded that the site reactivity of the present catalytic system competes favorably with the La_2O_3/Al_2O_3 (9) and Co/ZSM5 (4) systems. This important result has triggered further investigations of the La_2O_3/CaO system toward lean-NO_x performance by preparing small La_2O_3 crystallites deposited on CaO or vice versa with the coexistence also of other catalytic components. Results from these investigations are in progress in our laboratory.

Table 5 reports activity results per gram basis for the present reaction on the best alkaline- and rare-earth metal oxides reported in the literature. Results for the Co/ZSM5 system are also given for comparison. An accurate evaluation of the activity values given in Table 5 is rather difficult to be made mainly due to the different feed conditions used by the authors. It is noted that the Y_2O_3 catalyst with 80 m^2/g BET area is only about 2 times more active (after correcting for the NO partial pressure) than the present 5% La_2O_3/CaO solid with about 10 m^2/g BET area. This result implies that the site reactivity of the present catalytic system is significantly larger than that of Y_2O_3 catalyst.

4.5. *Effects of CH_4 and H_2 Pretreatment on the Adsorption and TPD Behavior of NO*

The 5 wt% La_2O_3/CaO sample has shown a dramatic increase in the uptake of NO following CH_4 or H_2 pretreatment, while the other three samples exhibit either no change or a significant decrease in the uptake of NO. It has been reported (16) that at $T > 600$°C CH_4 reacts with the surface lattice oxygen of CaO and La_2O_3 to form CO_2 and H_2O, while at $T > 400$°C the La_2O_3 surface is reduced by H_2. The effect of CH_4 pretreatment on the NO TPD was very minor in quantity and quality in the case of La_2O_3 but not in the case of CaO and 80 wt% La_2O_3/CaO samples. For La_2O_3, specific oxygen vacancies created by the reaction of methane or H_2 with the lattice oxygen are not offered for NO adsorption, while in the case of 5 wt% La_2O_3/CaO these sites do adsorb NO. The effect of CH_4 pretreatment on lanthana was to create sites of lower binding energy for NO chemisorption at the expense of sites of higher binding energy. An explanation to this behavior is that at 800°C surface diffusion of lattice oxygen toward vacant sites is possible, which is in agreement with theoretical studies (29).

Pure CaO and 80 wt% La_2O_3/CaO surfaces have shown a considerable decrease in their uptake of NO when pretreated with CH_4 or H_2. This result can be explained by arguing that CH_4 and H_2 remove surface oxygen species necessary for NO chemisorption according to Scheme 1. The fact that CH_4 pretreatment largely enhances the NO chemisorption on the 5 wt% La_2O_3/CaO, while the opposite is true on the 80 wt% La_2O_3/CaO, offers an additional explanation to their large catalytic activity differences observed (Fig. 2).

4.6. *Desorption of NO in the Presence of Gaseous CH_4 or O_2*

The large changes in the desorption kinetics of NO observed in the TPSR experiments with CH_4/He (Fig. 10) and O_2/He (Fig. 11), to be compared to the desorption kinetics observed in He flow (Fig. 3), are due only to chemical and not to mass transport effects. This is strongly supported by the TPDs of NO obtained in He and Ar flow described in the Results section. Isotopic exchange experiments with CH_4/CD_4 mixture have shown that methane can reversibly be activated on lanthana at $T > 600$°C (39). This activation leads to a splitting of the C–H bond and the formation of the C–D bond. It is generally agreed that this heterolytic splitting of the C–H bond proceeds on a M^{n+}–O^{2-} pair (M^{n+} = metal cation) (40). Based on this information, the effect of the presence of gaseous CH_4 on the desorption behavior of NO during TPSR can be stated as follows. At relatively low temperatures, there is only a weak interaction of CH_4 with the surface pair site M^{n+}–O^{2-}, which leads to a "zero" accumulation of adsorbed methane on the surface. However, this dynamic interaction of methane with the surface can influence the adsorption

and desorption processes of other molecules present in the gas and on the surface. It is known that readsorption phenomena during TPD studies from porous catalysts cannot be neglected. These phenomena can lead to an increase of the T_M value and also to a change in the shape of the TPD response (41). Therefore, one likely cause of the shift to lower desorption temperatures of NO in the presence of CH_4 is the decrease of the rate of readsorption of NO because of the weak interaction of CH_4 with the same sites for NO chemisorption. The formation of $H_3C^{\delta-}$–$H^{\delta+}$ dipole (due to the M^{n+}–O^{2-} pair site) can cause repulsive interactions with adjacent negatively charged adsorbed NO species. As a result of this, weakening of the *M*–O or N–O bonds in the adsorbed NO structure is possible and desorption of NO can occur at lower temperatures. In the case of O_2/He TPSR experiments, it is suggested that as the NO desorbs from the surface oxygen vacant sites become available for O_2 adsorption to form negatively charged oxygen species (33). These species can cause weakening of the bonding of the various negatively charged nitric oxide species. As a result of this, desorption of NO in O_2/He flow occurs at lower temperatures as compared to the case of He flow.

5. CONCLUSIONS

The following conclusions can be derived from the results of the present work:

1. Adsorption of NO at room temperature on pure CaO and La_2O_3 as well as on *x* wt% La_2O_3/CaO ($x = 5$ and 80 wt%) solids produces at least three kinds of adsorbed NO species as revealed by TPD experiments. This result is consistent with infrared studies of NO adsorption on CaO and La_2O_3 reported in the literature.

2. The amount of NO chemisorption on the 5 wt% La_2O_3/CaO solid measured after adsorption at 400°C followed by cooling in NO/He flow to room temperature does not follow the mixing rule, as opposed to the case of NO chemisorption at room temperature. For the former case, a significant increase in the number of activated adsorption sites per gram basis has been observed. It is suggested that this is largely due to doping of La_2O_3 by Ca^{2+} ions, thus creating oxygen vacancies that promote activated NO chemisorption. In the case of 80 wt% La_2O_3/CaO, the opposite NO chemisorption behavior obtained is likely due to the presence of sites formed by the doping of CaO by La^{3+} ions that inhibit NO adsorption.

3. Preadsorbed CO_2 on the surface of the La_2O_3/CaO system strongly inhibits the adsorption of NO. Part of preadsorbed CO_2 exchanges with NO at room temperature, while the nonexchangeable CO_2 strongly influences the desorption kinetics of NO.

4. The desorption kinetics of NO in a TPD experiment on the *x* wt% La_2O_3/CaO solids is strongly influenced by the presence of gaseous CH_4 and O_2. Lower desorption temperatures are observed as compared to the case of a TPD in He flow due to the presence of lateral repulsive interactions of weakly adsorbed $H_3C^{\delta-}-H^{\delta+}$ or negatively adsorbed oxygen species with negatively charged adsorbed nitric oxide species.

5. The binding energy of adsorbed oxygen species on the *x* wt% La_2O_3/CaO system decreases with increasing La_2O_3 content, while the amount of O_2 chemisorption goes through a maximum with increasing lanthana content. This behavior is influenced by the concentration and kinds of oxygen vacancies formed by the doping of La_2O_3 with Ca^{2+} ions.

6. The present work has provided fundamental information that can be used to explain the different catalytic activity behavior observed on the *x* wt% La_2O_3/CaO solids toward reduction of NO by CH_4 in the presence of excess O_2. The 5 wt% La_2O_3/CaO exhibits the highest rate of NO conversion per gram basis and site reactivity (TOF) at 550°C, while the 80 wt% La_2O_3/CaO the lowest rate. This behavior is related to (a) the higher surface coverage of adsorbed NO and oxygen species, (b) the lower amount of chemisorbed CO_2 in the presence of adsorbed NO, and (c) the increased amount and/or reactivity of new sites (oxygen vacancies) formed on the 5 wt% La_2O_3/CaO system.

ACKNOWLEDGMENTS

Financial support by the Research Committee of the University of Cyprus is gratefully acknowledged. We thank Dr. Ioannis Pashalides of the University of Cyprus for carrying out the BET surface area determinations of the *x* wt% La_2O_3/CaO samples. We are also grateful to Prof. P. G. Koutsoukos of the University of Patras (Greece) for performing the XRD and SEM analyses over the same samples.

REFERENCES

1. Held, W., Konig, A., Richter, T., and Puppe, L., SAE paper No. 900496 (1990).
2. Iwamoto, M., "Proc. Meet. Catal. Technol. Removal of NO," Tokyo, p. 17, Jan. 1990.
3. Fritz, A., and Pitchon, V., *Appl. Catal. B* **13**, 1 (1997).
4. Zhang, X., Walters, A. B., and Vannice, M. A., *J. Catal.* **155**, 290 (1995).
5. Zhang, X., Walters, A. B., and Vannice, M. A., *Appl. Catal. B* **4**, 237 (1994).
6. Zhang, X., Walters, A. B., and Vannice, M. A., *J. Catal.* **146**, 568 (1994).
7. Vannice, M. A., Walters, A. B., and Zhang, X., *J. Catal.* **159**, 119 (1996).
8. Zhang, X., Walters, A. B., and Vannice, M. A., *Appl. Catal. B* **7**, 321 (1996).
9. Shi, C., Walters, A. B., Vannice, M. A., *Appl. Catal. B* **14**, 175 (1997).
10. Fliatoura, K. D., Verykios, X. E., Costa, C. N., and Efstathiou, A. M., *J. Catal.* **183**, 323 (1999).
11. Fokema, M. D., and Ying, J. Y., *Appl. Catal. B* **18**, 71 (1998).
12. Belessi, V. C., Costa, C. N., Bakas, T. V., Anastasiadou, T., Pomonis, P. J., and Efstathiou, A. M., *Catal. Today* **59**, 347 (2000).
13. Anastasiadou, T., Loukatzikou, L., Costa, C. N., and Efstathiou, A. M., Submitted for publication.
14. Stockwell, D. M., Chung, J. S., and Bennett, C. O., *J. Catal.* **112**, 135 (1988).

15. Efstathiou, A. M., and Verykios, X. E., *Appl. Catal. A* **151**, 109 (1997), and references therein.
16. Papageorgiou, D., Ph.D. thesis, University of Patras, 1996.
17. Rieck, J. S., and Bell, A. T., *J. Catal.* **85**, 143 (1984).
18. Kortüm, G., and Quabeck, H., *Ber. Bunsenges. Phys. Chem.* **73**, 1020 (1969).
19. Low, M. J. D., and Yang, R. T., *J. Catal.* **34**, 479 (1974).
20. Hoost, T. E., Otto, K., and Laframboise, K. A., *J. Catal.* **155**, 303 (1995).
21. Klingenberg, B., and Vannice, M. A., *Chem. Mater.* **8**, 2755 (1996).
22. Klingenberg, B., and Vannice, M. A., *Appl. Catal. B: Envir.* **21**, 19 (1999).
23. Hansen, P. F. B., Dam-Johansen, K., Johnsson, J.-E., and Hulgaard, T., *Chem. Eng. Sci.* **47**, 2419 (1992).
24. Meubus, P., *J. Electrochem. Soc.* **124**, 49 (1977).
25. Winter, E. R. S., *J. Catal.* **22**, 158 (1971).
26. Vannice, M. A., Hyun, S. H., Kalpacki, B., and Liauh, W. C., *J. Catal.* **56**, 358 (1979).
27. Che, M., and Tench, A. J., *Adv. Catal.* **31**, 77 (1982).
28. Cerruti, L., Modone, E., Guglielminotti, E., and Borello, E., *J. Chem. Soc. Faraday Trans. 1* **70**, 729 (1974).
29. Ilett, D. J., and Islam, M. S., *J. Chem. Soc. Faraday Trans. 1* **89**, 3833 (1993).
30. Zhang, Z., Verykios, X. E., and Baerns, M., *Catal. Rev. Sci. Eng.* **36**(3), 507 (1994).
31. Lacombe, S., Geantet, C., and Mirodatos, C., *J. Catal.* **151**, 439 (1994).
32. Anderson, J. A., and Rochester, C. H., *J. Chem. Soc. Faraday Trans. 1* **82**, 1911 (1986).
33. Okonkwo, J., Ph. D. thesis, The University of West London, Uxbridge, U.K., 1992.
34. Bernal, S., Botana, F. J., Garcia, R., and Rodríguez-Izquierdo, J. M., *React. Solids* **4**, 23 (1987).
35. Rosynek, M. P., *Catal. Rev. Sci. Eng.* **16**, 111 (1977).
36. Bernal, S., Botana, F. J., Garcia, R., and Rodríguez-Izquierdo, J. M., *Thermochim. Acta* **66**, 139 (1983).
37. Yang, T., Feng, L., and Shen, S., *J. Catal.* **145**, 384 (1994).
38. Imai, H., Tagawa, T., and Kamide, N., *J. Catal.* **106**, 394 (1987).
39. Lacombe, S., Zanthoff, H., and Mirodatos, C., *J. Catal.* **155**, 106 (1995).
40. Sokolovskii, V. D., and Manedov, E. A., *Catal. Today* **13**(3), 419 (1992).
41. Gorte, R. J., *J. Catal.* **75**, 164 (1982).
42. Li, Y., and Armor, J. N., *Appl. Catal. B* **2**, 239 (1993).